ARTICLES
PUBLISHED ONLINE: 16 DECEMBER 2012 | DOI: 10.1038/NCHEM.1527
nature chemistry

Sulfur as a selective 'soft' oxidant for catalytic methane conversion probed by experiment and theory

Qingjun Zhu[1], Staci L. Wegener[1], Chao Xie[1], Obioma Uche[2], Matthew Neurock[2]* and Tobin J. Marks[1]*

Developing efficient catalytic processes to convert methane into useful feedstocks relies critically upon devising new coupling processes that use abundant, thermodynamically 'mild' oxidants together with selective catalysts. We report here on elemental sulfur as a promising 'soft' oxidant for selective methane conversion to ethylene over MoS_2, RuS_2, TiS_2, PdS and Pd/ZrO_2 catalysts. Experiments and density functional theory reveal that methane conversion is directly correlated with surface metal–sulfur bond strengths. Surfaces with weakly bound sulfur are more basic and activate methane C–H bonds more readily. In contrast, experimental and theoretical selectivities scale inversely with surface metal–sulfur bond strengths, and surfaces with the strongest metal–sulfur bonds afford the highest ethylene selectivities. High CH_4/S ratios, short contact times and the provision of a support maximizes the coupling of CH_x intermediates and selectivity to ethylene, because these conditions yield surfaces with stronger metal–sulfur bonding (for example, $Pd_{16}S_7$), which suppresses the over-oxidation of methane.

The anticipated long-term decline in petroleum reserves coupled with increasing worldwide energy demands will require alternative hydrocarbon feedstocks and conversion processes to produce fuels and basic chemical intermediates such as ethylene and propene[1]. Methane, the principal component of natural gas, is proposed as a suitable alternative because of its abundant reserves and high hydrogen:carbon ratio[2–4]. Although methane steam reforming to give synthesis gas ($CO + H_2$)[5,6]—followed by catalytic conversion to methanol and other oxygenates[7,8] or Fischer–Tropsch synthesis[9]—is widely practised, these routes are highly capital-intensive. A direct, high-selectivity, one-step route for the methane-to-olefins process would therefore be highly desirable.

Significant methane reserves are currently found in 'stranded' locations, and utilizing these reserves will require strategies for their efficient conversion to higher-value and/or more transportable products[10]. Indeed, for methane to be a viable carbon feedstock, more selective, less capital-intensive conversion processes are needed—a true 'grand challenge'[11]. To date, approaches explored for the direct, large-scale chemical transformation of methane to useful chemicals include aromatization[12], oxyclorination[13,14] and oxidative coupling[15]. However, these processes all have recognized limitations, including modest selectivities and yields, the requirement for corrosive reagents, heat management and temperature control, and/or dependence on toxic halogenated intermediates.

The seemingly straightforward oxidative transformation of methane with O_2 is in principle an attractive approach[15]; however, the yields to desired products are typically limited by severe over-oxidation pathways. Desired targets such as methanol, formaldehyde and ethylene are far more reactive with O_2 than methane, and are therefore rapidly converted into more thermodynamically stable products, principally CO_2. Furthermore, the reactions with O_2 are highly exothermic, and can increase local temperatures within reactors by 150–300 °C, thereby presenting significant heat management and reactor design issues. New catalytic strategies to enhance the selective conversion of methane to olefins or to other value-added intermediates with lower heat emission are therefore pivotal to developing viable methane conversion processes[16–23].

In comparison to O_2, the thermodynamic driving force for methane over-oxidation by S_2 is significantly less (it is a 'softer' oxidant; see Table 1 for a thermodynamic comparison of O_2 and S_2 as oxidants)[24,25]. This result arises primarily from the weaker C–S and H–S bonds and the lower bond enthalpies of the expected intermediates and products in comparison with those involving O_2. Note that the vapour-phase oxidative coupling of methane by sulfur (as gaseous S_2) to produce ethylene is entropically driven, and is exergonic only at temperatures above 950 K (Table 1, reaction 6). The use of sulfur as the oxidant in methane conversion may alleviate engineering issues associated with the significant local temperature excursions

Table 1 | Thermodynamic comparison of O_2 versus S_2 as oxidants for oxidative methane reactions at 1,073 K and 1,323 K.

	Oxygen oxidation processes	$\Delta G°$ (kJ mol^{-1})
(1)	$2CH_4 + O_2 \rightarrow C_2H_4 + 2H_2O$	−307 (−313*)
(2)	$2CH_4 + ½O_2 \rightarrow C_2H_6 + H_2O$	−117 (−104*)
(3)	$CH_4 + ½O_2 \rightarrow CH_3OH$	−75.3 (−62.3*)
(4)	$CH_4 + 2O_2 \rightarrow CO_2 + 2H_2O$	−792 (−797*)
(5)	$C_2H_4 + 3O_2 \rightarrow 2CO_2 + 2H_2O$	−1,294 (−1,286*)
	Sulfur oxidation processes	**$\Delta G°$ (kJ mol^{-1})**
(6)	$2CH_4 + S_2 \rightarrow C_2H_4 + 2H_2S$	−4.90 (−15.1*)
(7)	$2CH_4 + ½S_2 \rightarrow C_2H_6 + H_2S$	+33.9 (+45.1*)
(8)	$CH_4 + ½S_2 \rightarrow CH_3SH$	+35.5 (+46.0*)
(9)	$CH_4 + 2S_2 \rightarrow CS_2 + 2H_2S$	−124 (−145.3*)
(10)	$C_2H_4 + 3S_2 \rightarrow 2CS_2 + 2H_2S$	−236 (−235*)

*ΔG value at 1,323 K.

[1]Department of Chemistry and the Center for Catalysis and Surface Science, Northwestern University, Evanston, Illinois 60208-3113, USA, [2]Departments of Chemical Engineering and Chemistry University of Virginia, Charlottesville, Virginia 22904-4741, USA. *e-mail: t-marks@northwestern.edu; Neurock@virginia.edu

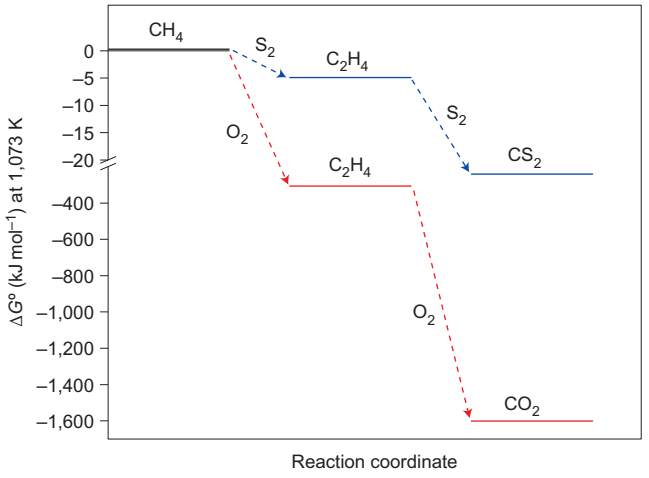

Figure 1 | Thermodynamic calculations show that using gaseous sulfur (S_2) as a 'soft' oxidant can hinder the over-oxidation of methane when compared with using O_2 as the oxidant. Comparison of the reaction thermodynamics for methane oxidative coupling to ethylene and over-oxidation by S_2 (blue) and O_2 (red), at 1,073 K, to undesired by-products.

that occur when O_2 is used. The thermodynamic data show that selective catalytic oxidative coupling of methane by S_2 should be possible if methane can be activated selectively. Note that the over-oxidation of methane to CS_2 or other species (Table 1, reactions 7–10) is far less favourable than the analogous over-oxidation by O_2 (Table 1, reactions 2–5), as summarized graphically in Fig. 1.

There is an extensive body of information concerning catalyst structure and reactivity[26–29] for the industrial desulfurization of hydrocarbons over transition-metal sulfides such as Co/MoS_2 and RuS_x catalysts[30–35]. However, very few studies have reported catalytic reactions involving elemental sulfur and saturated hydrocarbons[36,37]. Here, we report on the catalytic conversion of methane to ethylene (as expressed in reaction 6 of Table 1), using elemental sulfur as an oxidant over transition-metal sulfide catalysts. Experimental results indicating promising selectivity are used together with first-principles quantum chemical calculations to show that both the activation of methane and the selectivity of the subsequent conversion to ethylene can be linearly correlated with the catalyst metal–sulfur (M–S) bond strength (defined here as the energy to remove atomic sulfur as H_2S from the sulfide surface, using H_2), and that the two relationships are inversely related to one another. The sites that are most active for methane activation involve weakly bound surface sulfur atoms, which promote hydrogen abstraction, whereas those that are most selective involve strongly bound surface sulfur atoms, which facilitate hydrocarbon fragment coupling to C_2 products and suppress the over-oxidation of methane. Higher methane:sulfur (CH_4/S) feed ratios and higher temperatures enhance methane conversion and ethylene selectivity, and at the same time appear to reduce the active sulfide catalysts and increase the metal:sulfur compositions at the surface. This in turn decreases overall conversion while increasing the selectivity to ethylene. These insights demonstrate that sulfur is a promising reagent for the selective oxidative transformation of methane and should help guide the discovery of even more selective catalytic materials. The highest methane-to-ethylene selectivity is found here for supported PdS_x catalysts operating at relatively high temperatures, high CH_4/S ratios and short contact times.

Results and discussion

Catalytic reactions were carried out in a flow reactor specially designed to generate gaseous sulfur[38] as S_2 for reactions with hydrocarbons, using argon as the balance gas (see Supplementary Section A1 for details). Figure 2 presents a summary of methane conversion and ethylene selectivity data as a function of temperature over a series of catalysts. Note that these reactions are very clean and the only detectable carbon-containing products observed in the effluent stream are ethylene and carbon disulfide. Control experiments included blank reactions in quartz chip-packed reactor tubes. Passing methane through the reactor at 1,173 K in the absence of sulfur produces negligible amounts of ethylene. Although the reactions are carried out at relatively high temperatures, there is no evidence of significant coke formation on the catalyst surfaces after reaction, as assayed by UV–Raman spectroscopy[39] and combustion analysis (for a spent PdS catalyst operated for 4 h at 1,273 K, $C \leq 0.03$ wt%), and the mass balance in these processes is invariably >98%. Both methane conversion and ethylene selectivity (reported as two times the moles of ethylene produced/moles of methane reacted) increase markedly with increasing reaction temperature for all catalysts examined. The selectivity for ethylene is also strongly catalyst-dependent (Fig. 2b), following the trend $PdS > TiS_2 > RuS_2 > MoS_2$. PdS shows the highest ethylene selectivity, nearing 18% at 1,323 K, with methane conversion and ethylene selectivity

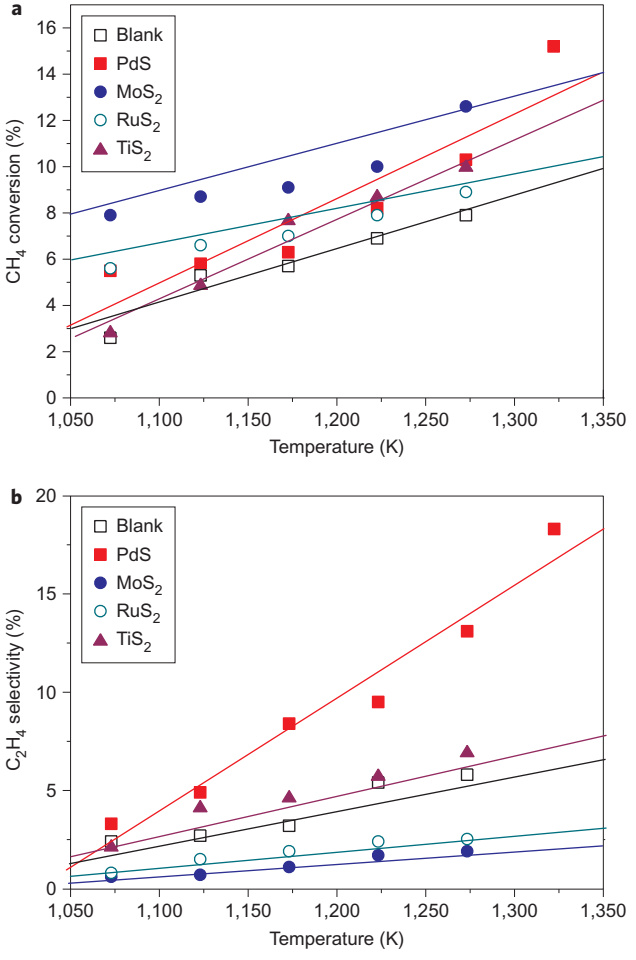

Figure 2 | Unsupported metal sulfides are effective catalysts for the conversion of methane to ethylene using gaseous sulfur as a 'soft' oxidant. **a**,**b**, Methane conversion (**a**) and ethylene selectivity (**b**) as a function of temperature over the indicated transition-metal sulfide catalysts. Reaction conditions for all metal sulfide catalysts: 5% CH_4 concentration in Ar; CH_4/S ratio = 5.8; overall WHSV = 30,000 ml g^{-1} h^{-1}. Estimated uncertainties in data points are ±5% of the stated value, and the straight lines are drawn as a guide to the eye.

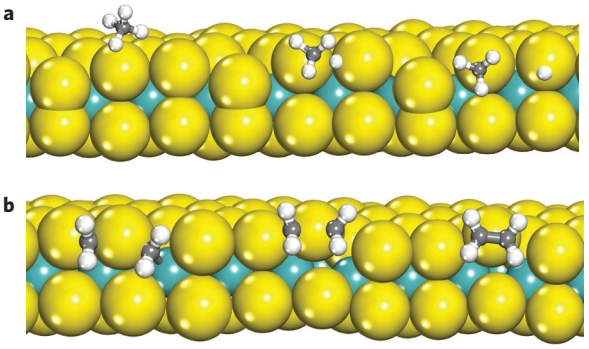

Figure 3 | *Ab initio* DFT calculations shows the characteristic reactant, transition state and product structures for the catalytic conversion of methane to ethylene using gaseous sulfur as the oxidant. a,b, Optimized reactant, transition state and product structures for the initial C–H activation of methane over surface S–S pairs (**a**) and CH_2 coupling to form ethylene at the sulfur edge of the MoS_2 surface (**b**). Similar structures are shown in the Supplementary Information for these same reactions at S–S sites on model RuS_2, PdS and TiS_2 surfaces. Yellow, sulfur; light blue, Pd; white, H; grey, C.

substantially higher with rising temperatures. In contrast, both the RuS_2 and MoS_2 catalysts exhibit very low ethylene selectivities—lower than the selectivity measured in the 'blank' experiments over the entire temperature range—because they efficiently catalyse over-oxidation to CS_2. A minimal ethylene yield is observed for all catalysts at temperatures below ~1,073 K. The absence of detectable ethane and methanethiol formation over any of the catalysts is in agreement with thermodynamic expectations that the formation of these products is unfavourable under these conditions (Table 1).

CH_x coupling can conceivably occur either on the surface of the catalyst or in the gas phase. The increased selectivity and conversion with increasing temperature reported in Fig. 2 in principle supports both surface as well as gas-phase CH_x coupling pathways, because increasing the temperature or conversion will increase CH_x species formation on the surface as well as in the gas phase. The increase in selectivity that occurs when using less active catalysts, however, would indicate that, regardless of where the actual CH_x coupling takes place, the key step involves CH_x–S* bond weakening to generate the active intermediates. Although we will explicitly discuss the coupling of CH_x–S* species on the surface, the results are essentially the same if the coupling occurs in the gas phase, as the desorption rate of $CH_3^{\cdot}$ radicals from the surface is inversely related to the CH_3–S* bond strength and linearly related to the M–S bond strengths.

First-principles density functional theory (DFT) calculations were carried out to help understand the reaction pathways and mechanisms, the nature of the active catalytic sites and the effects of the catalyst, as well as the reaction conditions on methane conversion and the selective formation of ethylene. Details concerning the computational methods used, as well as the results for the initial activation of methane, the subsequent C–H activation of other CH_x–S* intermediates, the coupling of surface hydrocarbon intermediates (CH_x–S*) to form ethylene, and the desorption of CH_x species from the surfaces are discussed in Supplementary Sections B1, B2. The coupling of CH_x intermediates was explored on the surface as well as in the gas phase.

Detailed structural optimizations were carried out on the close-packed 111, 100 and 110 surfaces of MoS_2, RuS_2, TiS_2 and PdS over a range of sulfur coverages to establish the lowest energy structures of the surfaces at different temperatures and CH_4/S ratios. The results for these model MoS_2, RuS_2, TiS_2 and PdS surfaces (shown in Supplementary Fig. S5) were used to determine the most favourable surface termination at specific sulfur chemical potentials and temperatures. As has been shown previously for methane oxidation, the chemical potential sets the composition of the surface as well as the nature of the active surface sites[40,41]. The lowest energy states and compositions for all of these structures were subsequently used to calculate the reaction energies and barriers for methane activation and the subsequent coupling of hydrocarbon fragments to form ethylene. These results suggest that under nearly all experimental conditions, MoS_2, RuS_2, TiS_2 and PdS are highly sulfided and the active sites comprise S–S pairs. The sole exception, as will be discussed below, occurs at high temperatures and high CH_4/S ratios where theory and experiment indicate that PdS is reduced to $Pd_{16}S_7$.

The rate of methane conversion is controlled by the activation of the initial CH_3–H bond, whereas catalytic selectivity for ethylene is controlled by the rate of coupling of two bound methylene (CH_2–S*) fragments to form ethylene versus the rate of further C–H bond activation to ultimately form CS_2. The calculated transition states for CH_3–H activation over S–S sites and the coupling of CH_2–S* fragments to form ethylene are shown in Fig. 3 and involve characteristic hydrogen abstraction and reductive C–C formation steps, respectively. Both reactions are strongly influenced by the M–S bond strength, which sets the basicity and reactivity of the surface sulfur sites. Weaker M–S bonds can readily abstract hydrogen and bind the resulting methyl groups more strongly, thus enhancing the activation of methane, whereas strong M–S bonds result in weaker C–S bonds, which enhance C–C coupling and increase the selectivity to form ethylene. The barriers for both the C–H bond activation of methane and the subsequent coupling of CH_2 surface intermediates to form ethylene appear to be linearly related to the M–S bond strength, as shown in Fig. 4.

The computed barriers for methane activation over the different metal sulfides reported in Fig. 4 increase with increasing M–S bond strength as $MoS_2 > RuS_2 \approx PdS > TiS_2$ and directly track the

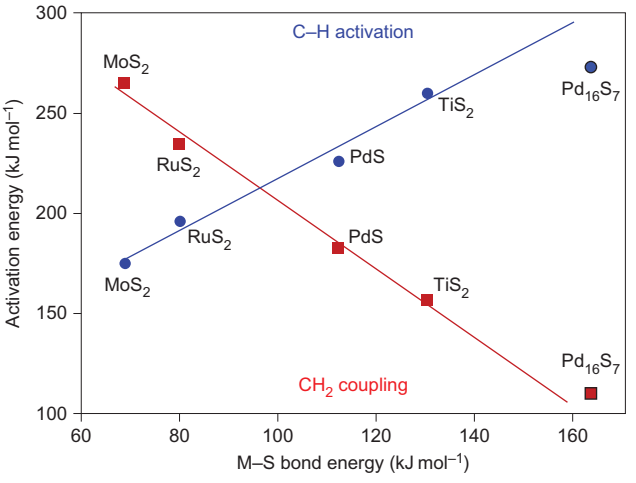

Figure 4 | Calculations reveal a correlation between both C–H activation and CH_2 coupling with M–S bond strength. The results from DFT quantum chemical calculations reveal a linear correlation between both the calculated activation barriers for methane C–H activation (blue) and the coupling of methylene (CH_2–S*) intermediates to form ethylene (red) with the corresponding M–S bond strength over S–S site pairs on model MoS_2, RuS_2, PdS, TiS_2 and $Pd_{16}S_7$ surfaces. The C–H activation and CH_2 coupling barriers over S–S sites on reduced $Pd_{16}S_7$ surfaces are indicated separately with larger symbols. The best fit lines and the corresponding values of the correlation coefficient (R) for methane activation (blue) and CH_2 coupling (red) are calculated to be E_a(C–H activation) = 100.27 ± 1.15 kJ mol^{-1} (M–S bond energy), $R = 0.990$; and E_a(CH_2 coupling) = 367.14 ± 1.60 kJ mol^{-1} (M–S bond energy), $R = 0.9958$, respectively.

experimental low-temperature conversion results in Fig. 2a. Although entropy has a significant effect on the reaction rate at high reaction temperatures, the changes in entropy that result from changes in the sulfide are very small and can be neglected without loss of generality. Methane activation is governed by a hydrogen abstraction, for which the reactant and transition-state structures for all of the sulfides examined were nearly identical.

Methane conversion is clearly governed by the M–S bond strength. Sulfides with weaker M–S bonds result in more basic and reactive sulfur sites that can readily abstract hydrogen in the transition state and bind the resulting CH_3 and hydrogen intermediates. Subsequent C–H activations of the resulting CH_x* species have lower activation barriers and more favourable activation entropies than those for methane, and are therefore more reactive. As such, metal sulfides with weaker M–S bonds will not only readily activate the C–H bond of methane, but will continue on to activate the C–H bonds of the subsequent CH_x fragments and ultimately mediate over-oxidation to CS_2. The calculations for C–H activation at CH_3*–S, CH_2*–S and CH*–S sites on MoS_2 yield barriers of 119, 63 and 178 kJ mol^{-1}, respectively, which are significantly lower than the initial 184 kJ mol^{-1} barrier for methane activation.

In contrast to these results, computed trends in the methane-to-ethylene selectivity are inversely related to M–S bond strength, as also shown in Fig. 4, where the barriers for ethylene formation decrease as $MoS_2 > RuS_2 > PdS > TiS_2$. These results are consistent with the experimental results shown in Fig. 2b at temperatures below 1,175 K, with the exception that PdS is only slightly more selective than TiS_2. Similar results for selectivity are found if the CH_3 radicals desorb from the surface and recombine in the gas phase to form ethane, because the CH_3 desorption barriers are linearly correlated with the CH_2–S* coupling barriers, as shown in Supplementary Fig. S12. The barriers to activate the C–H bonds of CH_3–S* intermediates and subsequently couple the CH_2–S* species to form ethylene are both lower than the barriers for CH_3 radical desorption, as shown in Supplementary Fig. S12. This suggests that CH_2–S* coupling on the surface is more favourable than the desorption and gas-phase coupling of CH_3 radicals.

A more detailed analysis of the C–H bond activation steps versus the CH_2–S*···CH_2–S* coupling reactions indicates that the M–S bond becomes sufficiently strong in PdS and TiS_2 to begin to reverse the driving force to over-oxidize to CS_2 and instead increases the likelihood of CH_2–S* coupling to form ethylene. On PdS, the barrier to CH_2–S* coupling to form ethylene is 183 kJ mol^{-1}, which is only 50 kJ mol^{-1} greater than the barrier to activate the C–H bond of CH_2–S* (134 kJ mol^{-1}). Note, however, that the change in entropy for CH_2–S* coupling is significantly more favourable than that for C–H bond activation. At higher temperatures, both steps become favourable. On TiS_2, the CH_2–S* coupling process is computed to be far more favourable than the C–H activation of CH_2–S* species.

Further examination of the experimental results in Fig. 2b indicates that although the selectivity to ethylene increases with increasing temperature for all of the sulfides, the results for PdS are characteristically different because the selectivity increases far more dramatically with temperature than for the other sulfides. As can be seen in Fig. 2a, there also appears to be a distinct change in the relative experimental ordering of methane activation over the different metal sulfides at temperatures above ~1,150 K. X-ray diffraction (XRD) data for the PdS catalyst before and after operation at high temperatures are shown in Supplementary Fig. S2A and compared with PDF (Powder Diffraction File) database spectra for PdS (Supplementary Fig. S2B) and $Pd_{16}S_7$ (Supplementary Fig. S2C). These data suggest that the bulk of the PdS is reduced to $Pd_{16}S_7$ under catalytic reaction conditions. Similar XRD characterization of the initial and spent MoS_2 catalysts

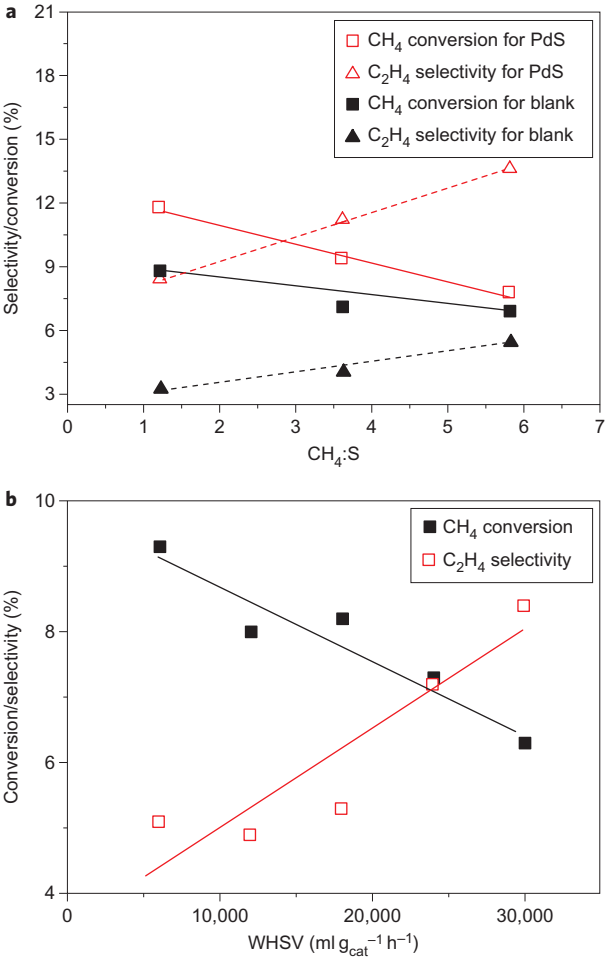

Figure 5 | Markedly altered PdS-catalysed methane conversion and ethylene selectivity are observed by varying the CH_4:S feed ratios and WHSVs over the catalyst surface. a,**b**, Effect of CH_4/S ratio (reaction conditions: temperature = 1,223 K, sulfur vapour concentration = 0.85%, overall WHSV = 30,000 ml g^{-1} h^{-1}) (**a**) and WHSV (reaction conditions: 1,173 K, 5% CH_4 concentration in Ar, CH_4/S ratio = 5.8) on methane conversion and ethylene selectivity over a PdS catalyst (**b**). Estimated uncertainties in data points are ±5% of the stated value, and the straight lines are drawn as a guide to the eye.

(Supplementary Fig. S3) reveals that these remain unchanged under all reaction conditions.

The CH_4/S ratio is found to be a critical parameter governing selectivity in the present catalytic conversions over PdS. The experimental results in Fig. 5a show that over-oxidation of methane to CS_2 is suppressed at high CH_4/S ratios, thereby enhancing ethylene selectivity. In reactant streams with CH_4/S ratios less than 1:1, ethylene formation is suppressed, and CS_2 is the only observed carbon-containing product. The dependence of selectivity on the CH_4/S ratio logically follows because over-oxidation is stoichiometrically more favourable at high oxidant concentrations. The increasing ethylene selectivity with increasing CH_4/S over PdS is consistent with the experimental results presented in Fig. 2b, which show a significant increase in selectivity with increasing temperature. Both higher temperatures and higher CH_4/S ratios lead to the reduction of PdS to $Pd_{16}S_7$. The results clearly show that the more reduced $Pd_{16}S_7$ state is less active but significantly more selective for ethylene. Similar phase changes between PdO and oxygen-covered Pd metal, and concomitant decreases in the rate of catalytic methane activation, have been

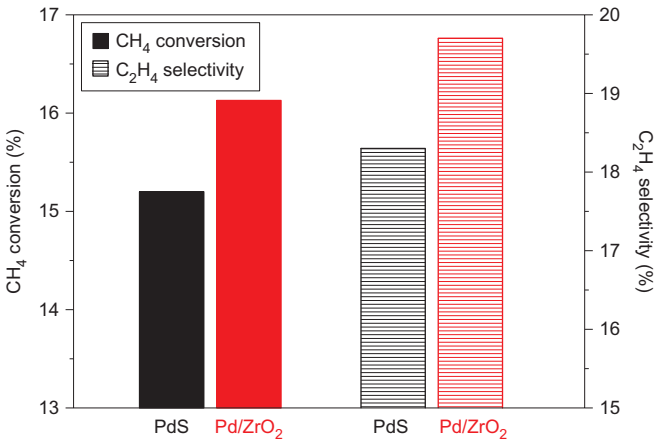

Figure 6 | A ZrO_2-supported palladium sulfide catalyst exhibits significantly enhanced catalytic performance compared with an unsupported catalyst in the conversion of methane to ethylene using gaseous sulfur as the oxidant. Comparison of methane conversion and ethylene selectivity over bulk PdS and supported Pd/ZrO_2 catalysts. Reaction conditions: 1,323 K, 5% CH_4 concentration in Ar, CH_4/S ratio = 5.8. Estimated uncertainties in the data are ±5% of the stated value.

reported for methane oxidation with increasing CH_4:O_2 ratios and temperatures[42].

To increase catalyst dispersion and possibly enhance catalytic performance, a ZrO_2-supported 10 wt% palladium catalyst (Pd/ZrO_2) was synthesized and evaluated. As can be seen in Fig. 6, both methane conversion and ethylene selectivity are significantly enhanced over those for bulk PdS, with ethylene selectivity now approaching 20%. Considering that the palladium loading in Pd/ZrO_2 catalysts is ~10% that of bulk PdS catalysts, we infer that Pd/ZrO_2 exhibits significantly higher efficiency in methane conversion to ethylene. Furthermore, examination using XRD indicates that the palladium in Pd/ZrO_2 is converted to $Pd_{16}S_7$ after ~2 h on stream (Supplementary Fig. S4B), in agreement with the observation that, after a short initial period, Pd/ZrO_2 catalytic performance is stable for at least 24 h (Supplementary Fig. S4A).

DFT-computed phase diagrams for $Pd_{16}S_7$ (Supplementary Fig. S15) indicate that higher temperatures and higher CH_4/S ratios result in stable sulfur-terminated 110 and 111 surfaces that expose Pd–S site pairs with M–S bond strengths of 167 kJ mol^{-1}, which is 55 kJ mol^{-1} greater than the M–S bond strengths on PdS. Despite the stronger M–S bonding, methane can be readily activated at the Pd–S sites in a four-centre transition state via a σ-bond metathesis-type mechanism (Supplementary Fig. S17) with a barrier of 166 kJ mol^{-1}. Although the initial methane molecule is activated at this site and continues to form CH_2*, the coupling of two CH_2* surface intermediates requires the activation of a second methane molecule at a vicinal S–S site pair. The large Pd–S bond strength at these vicinal S–S sites increases the methane activation barriers at these sites to 241 kJ mol^{-1} (Supplementary Fig. S16), which is 34 kJ mol^{-1} greater than for the Pd–S bonds present on the PdS surface. These strong M–S bonds also significantly weaken the CH_2–S* bonding and lower the barriers for subsequent coupling of the CH_2–S* intermediates to form ethylene (Supplementary Fig. S18) to only 103 kJ mol^{-1}, which is 80 kJ mol^{-1} lower than that on PdS. This situation significantly enhances the selectivity to ethylene on the reduced $Pd_{16}S_7$ surface compared with that on the other metal sulfides examined, and raises important implications for future catalyst design.

The resulting C–H activation and CH_2–CH_2 coupling barriers over the $Pd_{16}S_7$ surface S–S pairs track very closely the aforementioned linear correlation with M–S bond strength, and are plotted together with the barriers for all the highly sulfided surfaces in Fig. 4. The resulting barriers are fully consistent with the experimental results, showing that the $Pd_{16}S_7$ catalytic material has lower activity than the other sulfides but proceeds with markedly higher selectivity to ethylene at higher temperatures (Fig. 1) and at higher CH_4/S ratios (Fig. 5).

To better understand the methane over-oxidation pathways in the present catalytic systems, methane conversion and ethylene selectivity over the PdS catalysts were also studied as a function of weight hour space velocity (WHSV; Fig. 5b). At high WHSV, where the residence time in the catalyst bed is short, selectivity to ethylene is significantly enhanced, but over-oxidation to CS_2 becomes more pronounced at longer residence times and is reasonably attributable to follow-up reactions of ethylene with S_2 to form CS_2. This scenario was verified in control experiments.

Conclusions

The results reported here demonstrate that sulfur is a promising 'soft' oxidant for the heterogeneous catalytic conversion of methane to ethylene because the M–S bonds are significantly stronger than the M–O bonds in the corresponding O_2 oxidations. Lower (more controlled) conversions of methane as well as higher selectivities of methane to ethylene conversion are observed here on sulfides with the strongest surface M–S bonds. High CH_4/S ratios and high WHSVs promote favourable conversion selectivity to ethylene and suppress undesired over-oxidation pathways. MoS_2, RuS_2, TiS_2 and PdS are effective catalysts for methane conversion to ethylene and/or CS_2 using sulfur as the oxidant. However, activity and selectivity are strongly catalyst-dependent, with the partially reduced PdS in the form of bulk or ZrO_2-supported $Pd_{16}S_7$ exhibiting the highest selectivity. Although the selectivities to ethylene in these preliminary experiments are currently modest, it is likely that they will be increased substantially following optimization of conditions and catalysts. These results demonstrate that metal sulfides and, more generally, transition-metal chalcogenides, offer the ability to substantially control the conversion and selective oxidation of methane to ethylene by sulfur. Furthermore, using S_2 as the oxidant rather than O_2 should suppress the dramatic temperature excursions that occur in oxidative methane coupling with O_2, because the S_2 reactions are nearly thermoneutral. This should therefore relax engineering constraints associated with heat removal. Note also that the H_2S produced in the present catalytic coupling can be used to regenerate the sulfur feedstock by means of the efficient, industrially practised Claus process[43]:

$$2H_2S + O_2 \rightarrow S_2 + 2H_2O$$

In essence, sulfur serves in the present approach as a redox mediator for O_2 oxidation.

Methods

A custom heterogeneous catalytic reactor (fabricated by Altamira Instruments) was designed for using elemental sulfur as a gaseous reactant for the oxidative coupling of methane. Typical reactions were carried out between 1,073 and 1,323 K with a 5% methane stream, using argon as the balance gas. Blank tests were carried out under identical reaction conditions using an empty reactor filled with quartz chips. The metal sulfide catalysts MoS_2, TiS_2, RuS_2 and PdS were purchased from Sigma-Aldrich and Alfa Aesar, and were used without further purification. The WHSV was varied between 6,000 and 30,000 ml h^{-1} g^{-1} by adjusting the amount of catalyst in the reactor from 500 to 100 mg. All the reactions were carried out under ambient pressure. Reaction products were monitored online and quantified using a gas chromatograph with flame photometric detection (FPD), thermal conductivity detection (TCD) and flame ionization detection (FID) detectors. A more detailed description of the reaction setup and catalyst characterization is provided in Supplementary Sections A1, A2.

Received 1 August 2012; accepted 8 November 2012; published online 16 December 2012

References

1. Tullo, A. H. Celanese takes an ethanol plunge. *Chem. Eng. News* **89,** 20–21 (2011).
2. Crabtree, R. H. Aspects of methane chemistry. *Chem. Rev.* **95,** 987–1007 (1995).
3. Lunsford, J. H. Catalytic conversion of methane to more useful chemicals and fuels: a challenge for the 21st century. *Catal. Today* **63,** 165–174 (2000).
4. Holmen, A. Direct conversion of methane to fuels and chemicals. *Catal. Today* **142,** 2–8 (2009).
5. Horn, R., Williams, K. A., Degenstein, N. J. & Schmidt, L. D. Syngas by catalytic partial oxidation of methane on rhodium: mechanistic conclusions from spatially resolved measurements and numerical simulations. *J. Catal.* **242,** 92–102 (2006).
6. York, A. P. E., Xiao, T. C., Green, M. L. H. & Claridge J. B. Methane oxyforming for synthesis gas production. *Catal. Rev. Sci. Eng.* **49,** 511–560 (2007).
7. Bar-Nahum, I., Khenkin, A. M. & Neumann, R. Mild, aqueous, aerobic, catalytic oxidation of methane to methanol and acetaldehyde catalyzed by a supported bipyrimidinylplatinum–polyoxometalate hybrid compound. *J. Am. Chem. Soc.* **126,** 10236–10237 (2004).
8. Otsuka, K. & Wang, Y. Direct conversion of methane into oxygenates. *Appl. Catal. A* **222,** 145–161 (2001).
9. Dry, M. E. Practical and theoretical aspects of the catalytic Fischer–Tropsch process. *Appl. Catal. A* **138,** 319–344 (1996).
10. Flores, R. M. Coalbed methane: from hazard to resource. *Int. J. Coal Geol.* **35,** 3–26 (1998).
11. DOE Basic Energy Sciences Advisory Committee. *Directing Matter and Energy: Five Challenges for Science and the Imagination* (National Academy Press, 2007).
12. Xu, Y. D., Bao, X. H. & Lin, L. W. Direct conversion of methane under nonoxidative conditions. *J. Catal.* **216,** 386–395 (2003).
13. Podkolzin, S. G., Stangland, E. E., Jones, M. E., Peringer, E. & Lercher, J. A. Methyl chloride production from methane over lanthanum-based catalysts. *J. Am. Chem. Soc.* **129,** 2569–2576 (2007).
14. Peringer, E., Salzinger, M., Hutt, M., Lemonidou, A. A. & Lercher J. A. Modified lanthanum catalysts for oxidative chlorination of methane. *Top. Catal.* **52,** 1220–1231 (2009).
15. Zavyalova, U., Holena, M., Schlögl, R. & Baerns, M. Statistical analysis of past catalytic data on oxidative methane coupling for new insights into the composition of high-performance catalysts. *ChemCatChem* **3,** 1935–1947 (2011) and references therein.
16. Lang, S. M., Bernhardt, T. M., Barnett R. N. & Landman, U. Methane activation and catalytic ethylene formation on free Au^{2+}. *Angew. Chem. Int. Ed.* **49,** 980–983 (2010).
17. Sorokin, A. B. *et al.* Oxidation of methane and ethylene in water at ambient conditions. *Catal. Today* **157,** 149–154 (2010).
18. Periana, R. A. *et al.* Mercury-catalyzed, high-yield system for the oxidation of methane to methanol. *Science* **259,** 340–343 (1993).
19. Groothaert, M. H., Smeets, P. J., Sels, B. F., Jacobs, P. A. & Schoonheydt, R. A. Selective oxidation of methane by the bis(mu-oxo)dicopper core stabilized on ZSM-5 and mordenite zeolites. *J. Am. Chem. Soc.* **127,** 1394–1395 (2005).
20. An, Z. J., Pan, X. L., Liu, X. M., Han, X. W. & Bao, X. H. Combined redox couples for catalytic oxidation of methane by dioxygen at low temperatures. *J. Am. Chem. Soc.* **128,** 16028–16029 (2006).
21. Luzgin, M. V. *et al.* Understanding methane aromatization on a Zn-modified high-silica zeolite. *Angew. Chem. Int. Ed.* **47,** 4559–4562 (2008).
22. Palkovits, R., Antonietti, M., Kuhn, P., Thomas, A. & Schuth, F. Solid catalysts for the selective low-temperature oxidation of methane to methanol. *Angew. Chem. Int. Ed.* **48,** 6909–6912 (2009).
23. Gretz, E., Oliver, T. F. & Sen, A. Carbon–hydrogen bond activation by electrophilic transition-metal compounds—palladium(II)-mediated oxidation of arenes and alkanes including methane. *J. Am. Chem. Soc.* **109,** 8109–8111 (1987).
24. Linstrom, P. J. & Mallard, W. G. (eds) *NIST Chemistry WebBook; NIST Standard Reference Database Number 69* (National Institute of Standards and Technology, 2011). Available at http://webbook.nist.gov.
25. Stull, D. R., Westrum, E. F. & Sinke, G. C. *The Chemical Thermodynamics of Organic Compounds* 243–244 (Wiley, 1969).
26. Polyakov, M. *et al.* Mechanochemical activation of MoS_2—surface properties and catalytic activities in hydrogenation and isomerization of alkenes and in H_2/D_2 exchange. *J. Catal.* **260,** 236–244 (2008).
27. Chianelli, R. R., *et al.* Periodic trends in hydrodesulfurization: in support of the Sabatier principle. *Appl. Catal. A* **227,** 83–96 (2002).
28. Byskov, L. S., Norskov, J. K., Clausen, B. S. & Topsoe, H. DFT calculations of unpromoted and promoted MoS_2-based hydrodesulfurization catalysts. *J. Catal.* **187,** 109–122 (1999).
29. Besenbacher, F. *et al.* Recent STM, DFT and HAADF-STEM studies of sulfide-based hydrotreating catalysts: insight into mechanistic, structural and particle size effects. *Catal. Today* **130,** 86–96 (2008).
30. Corma, A., Martinez, C., Ketley, G. & Blair, G. On the mechanism of sulfur removal during catalytic cracking. *Appl. Catal. A* **208,** 135–152 (2001).
31. Kabe, T., Ishihara, A. & Qian, W. *Hydrodesulfurization and Hydrodenitrogenation: Chemistry and Engineering* (Wiley-VCH, 1999).
32. Chianelli, R. R. *et al.* Catalytic properties of single layers of transition metal sulfide catalytic materials. *Catal. Rev. Sci. Eng.* **48,** 1–41 (2006).
33. Topsoe, H., Clausen, B. S. & Massoth, F. E. in *Hydrotreating Catalysis—Science and Technology*, Vol. 11 (eds Anderson, J.R. & Boudart, M.) (Springer, 1996).
34. Bezverkhyy, I., Afanasiev, P., Geantet, C. & Lacroix, M. Highly active $(Co)MoS_2/Al_2O_3$ hydrodesulfurization catalysts prepared in aqueous solution. *J. Catal.* **204,** 495–497 (2001).
35. Wang, H. M. & Iglesia, E. Thiophene hydrodesulfurization catalysis on supported Ru clusters: mechanism and site requirements for hydrogenation and desulfurization pathways. *J. Catal.* **273,** 245–256 (2010).
36. Anderson, J. R., Chang, Y. F., Pratt, K. C. & Foger, K. Reaction of methane and sulfur—oxidative coupling and carbon-disulfide formation. *React. Kinet. Catal. Lett.* **49,** 261–269 (1993).
37. Didenko, L. P., Linde, V. R. & Savchenko, V. I. Partial catalytic oxidation and condensation of methane by oxygen and sulfur. *Catal. Today* **42,** 367–370 (1998).
38. Nehb, W. & Vydra, K. F. *Sulfur. Ullman's Encyclopedia of Industrial Chemistry* (Wiley-VCH, 2002).
39. Stair, P. C. The application of UV Raman spectroscopy for the characterization of catalysts and catalytic reactions. *Adv. Catal.* **51,** 75–98 (2007).
40. Chin, Y., Buda C., Neurock, M. & Iglesia, E. Reactivity of chemisorbed oxygen atoms and their catalytic consequences during CH_4/O_2 catalysis on supported Pt clusters. *J. Catal.* **283,** 10–24 (2011).
41. Chin, Y., Buda, B., Neurock, M. & Iglesia, E. Selectivity of chemisorbed oxygen in C–H bond activation and CO oxidation and kinetic consequences for CH_4–O_2 catalysis on Pt and Rh clusters. *J. Am. Chem. Soc.* **133,** 15958–15978 (2011).
42. Chin, Y. & Iglesia, E. Elementary steps, the role of chemisorbed oxygen, and the effects of cluster size in catalytic CH_4–O_2 reactions on palladium. *J. Phys. Chem.* **115,** 17845–17855 (2011).
43. Jüngst, E. & Nehb, W. *Handbook of Heterogeneous Catalysis* Ch. 12.4 (Wiley-VCH, 2008).

Acknowledgements

The authors thank the Dow Chemical Company for support as part of the Methane Challenge project. The authors thank S. Domke, P. Nickias, D. Barton and M. Kaminsky for stimulating discussions.

Author contributions

Q.Z., S.L.W. and C.X. performed the experiments, analysed the data, and wrote portions of the manuscript. O.U. and M.N. performed DFT calculations and wrote portions of the manuscript. All authors contributed to writing and revising the manuscript.

Additional information

Supplementary information is available in the online version of the paper. Reprints and permission information is available online at http://www.nature.com/reprints. Correspondence and requests for materials should be addressed to M.N. and T.J.M.

Competing financial interests

The authors declare no competing financial interests.